International Journal of Environmental Science and Technology (2025) 22:14383–14402
https://doi.org/10.1007/s13762-025-06564-5

ORIGINAL PAPER

Adsorption behavior of 17α-ethinylestradiol onto mesostructured calcium-based metal–organic frameworks adsorbent from water

F. F. Sukatis[1] · L. J. Looi[1] · H. N. Lim[2] · M. B. A. Rahman[2] · A. Z. Aris[1,3]

Received: 28 February 2024 / Revised: 13 April 2025 / Accepted: 3 May 2025 / Published online: 3 June 2025

Abstract

The removal of 17α-ethynylestradiol (EE2), a persistent endocrine-disrupting compound, from aqueous environments was investigated using three calcium-based metal–organic frameworks (Ca-MOFs): Ca-BDC, Ca-BTC, and Ca-MIX. The Ca-MOFs were synthesized and characterized using PXRD, FTIR, BET, and SEM. Batch adsorption experiments were conducted to evaluate the effect of solution pH, temperature, ionic strength, and humic acid concentration on EE2 removal. Kinetic studies were performed at an initial EE2 concentration of 10 µg/L using 50 mg of adsorbent at unadjusted (native) pH, analyzing adsorption over different contact times. Non-linear kinetic models were applied to interpret adsorption behavior. For isotherm studies, EE2 uptake was investigated across a range of initial concentrations (10–200 µg/L) under fixed conditions (50 mg adsorbent, 2 h contact time, native pH). Langmuir and Freundlich isotherm models were employed to describe the equilibrium data. Among the three adsorbents, Ca-MIX exhibited the highest EE2 adsorption capacity (52.03 µg/g), followed by Ca-BDC (35.69 µg/g) and Ca-BTC (19.49 µg/g). Adsorption followed the Langmuir isotherm and pseudo-second-order kinetic models, indicating monolayer chemisorption. Thermodynamic analysis revealed endothermic and spontaneous adsorption. The adsorption mechanism was primarily governed by hydrophobic interactions, electrostatic attraction, and hydrogen bonding. Increased humic acid concentration and extreme pH conditions significantly influenced adsorption behavior. The study demonstrates the potential of Ca-MOFs, especially Ca-MIX, as efficient adsorbents for EE2 removal. These findings contribute valuable insights into designing effective MOF-based adsorbents for water purification applications targeting micropollutants.

Keywords Endocrine-disrupting compounds · Calcium-based metal–organic frameworks · Adsorption

Introduction

Pharmaceutical and personal care products (PPCPs) encompass a broad spectrum of substances such as antibiotics, painkillers, hormone preparations, hair dyes, and skin care products. The presence of these substances in water sources is becoming an alarming issue as they are emerging as persistent and micropollutants. (Narayanan et al. 2022; Sun et al. 2019). These PPCPs are released from point sources and non-point sources into the aquatic environment due to insufficient treatment in water treatment technology (Xie et al. 2022). The metabolites of PPCPs have been shown to persist in the environment for several years, raising ecotoxicological risks (Couto et al. 2022). Furthermore, some PPCP compounds may never completely degrade and may persist indefinitely in the environment. Although PPCPs are typically found in trace concentrations in surface water, at levels between ng/L and µg/L, they can still pose a threat to exposed organisms and ecosystems (Peng et al. 2018; Xie et al. 2022). Synthetic hormones such as Ethinylestradiol (EE2) being particularly concerning due to its widespread use in medications including combinations found in oral contraceptive pills (Aris et al. 2014). The widespread use

Editorial responsibility: Samareh Mirkia.

✉ A. Z. Aris
zaharin@upm.edu.my

[1] Department of Environmental Science and Technology, Faculty of Forestry and Environment, Universiti Putra Malaysia, 43400 Serdang, Selangor, Malaysia

[2] Department of Chemistry, Faculty of Science, Universiti Putra Malaysia, 43400 Serdang, Selangor, Malaysia

[3] International Institute of Aquaculture and Aquatic Sciences, Universiti Putra Malaysia, 71050 Port Dickson, Negeri Sembilan, Malaysia

of EE2 for medical purposes has resulted in its accumulation in the environment. Consequently, there is an imminent necessity for the development of straightforward and highly efficient techniques for EE2 removal from the environment. Research has shown that EE2 can be found in freshwater systems, with concentrations reaching up to an average of 25,000 ng/L in some areas. Such elevated levels are often associated with regions impacted by wastewater discharge or agricultural runoff, where EE2 enters waterways and accumulates over time (de França et al. 2020; Tang et al. 2021; Almeida et al. 2020; López-Velázquez et al. 2021). EE2, a synthetic estrogen, exhibits potent endocrine-disrupting effects on aquatic organisms even at low concentrations. By interfering with hormone synthesis and regulation, EE2 induces physiological abnormalities, including the feminization of male fish, intersex conditions, and altered reproductive behaviors. Persistent exposure to EE2 further leads to reproductive and developmental impacts, such as reduced fertility, abnormal egg production, and skewed sex ratios, all of which contribute to cascading effects on population dynamics and community structures (Bókony et al. 2018; Martins et al. 2022; da Silva et al. 2022). Moreover, EE2's persistence in aquatic environments and its potential to bioaccumulate within food chains amplify its toxic effects on higher trophic levels, as evidenced by decreased reproductive success and other adverse outcomes (Clouzot et al. 2020). These impacts extend to ecosystem-wide consequences, including reductions in biodiversity, disruptions in species composition, and diminished ecological stability. The cascading effects of EE2 across multiple trophic levels highlight its long-term ecological risks, threatening the resilience and functionality of aquatic ecosystems.

Adsorption-based treatment technology is a commonly used approach for removing emerging compounds from the aqueous environment owing to its high efficiency and low cost (Aris et al. 2020). Metal–organic frameworks (MOFs) have been widely studied and synthesized worldwide due to their unique design, high porosity, and flexibility (Vakiti et al. 2012; Furukawa et al. 2013). Although MOFs have unique properties, there are concerns that limit their practical and commercial use. For example, the majority of MOFs are made of transition elements, which could result in instability when in contact with water, thus reducing their capacity and generating potentially harmful by-products. Therefore, the development of sustainable nanomaterials is critical to ensure the viability of MOFs-based adsorbents while improving their environmental compatibility, durability, and affordability (Sukatis and Aris 2021). Recent research has shown that MOFs possess outstanding adsorption performance and selectivity in eliminating various contaminants, including PPCPs. This performance is attributed to their unique structural features, such as high surface area, tunable porosity, and optimized pore size distribution, which enable efficient and selective adsorption of PPCPs. Specific examples include the selective removal of contaminants achieved through pore size optimization (Sukatis et al. 2024). The material composition of MOFs further contributes to their adsorption efficiency. Metal ions, such as Fe, Zr, and Cu, and functionalized organic linkers, such as carboxyl and amine groups, enhance adsorption through mechanisms like hydrogen bonding, π-π interactions, and electrostatic forces (Lee et al. 2024; Ahmed et al. 2023). The interplay between these structural and compositional attributes creates synergistic effects, where the integration of specific metal ions with functionalized linkers forms unique active sites that enhance both adsorption capacity and selectivity (Mishra et al. 2024). Notable examples of MOFs, such as UiO-66 and MIL-101, highlight these synergistic effects. Moreover, previous research has reported significant adsorption capacities of MOFs for endocrine-disrupting chemicals (EDCs), including PPCPs, ranging from 32 mg/g to 1100 mg/g (Li et al. 2020; Dehghan et al. 2019; Sarker et al. 2019; Jun et al. 2019). These results highlight the promise of MOFs as efficient adsorbent materials for use in environmental cleanup efforts. However, significant limitations, including the high costs associated with MOF synthesis, challenges in achieving uniform performance at a large scale, and difficulties in effective regeneration, hinder the overall cost-effectiveness of MOF-based treatment technologies (Khatoon et al. 2024; Zhang et al. 2022; Singh et al. 2024). These issues are particularly pronounced when compared to traditional methods such as activated carbon and membrane filtration, which offer more established scalability and regeneration processes. Additionally, concerns related to the stability of MOFs under variable environmental conditions, potential leaching of metal ions, and the environmental footprint of synthesis further highlight the need for innovative solutions to enhance the practicality and sustainability of MOF applications for contaminant removal. Therefore, the selection of raw materials for MOF synthesis should be carefully considered. Fortunately, alkaline earth elements are abundantly found in mineral deposits and offer ideal opportunities for developing environmentally friendly and cost-effective MOFs-based adsorbents (Li et al. 2019; Sumida et al. 2016; Wei et al. 2017; Sukatis et al. 2022). Alkaline earth metal-based MOFs, utilizing metals such as Magnesium and Calcium, are widely recognized for environmental friendliness, cost-effectiveness, and natural abundance, making these materials ideal for sustainable applications. The non-toxic and biodegradable nature of alkaline earth metal-based MOFs reduces ecological risks, and the simpler, less resource-intensive synthesis methods align with green chemistry principles. However, adsorption capacities and structural tunability of these MOFs are often lower, potentially requiring increased material usage or extended operational times for contaminant removal (Zang

et al. 2021; Ye et al. 2021). In contrast, transition metal-based MOFs, incorporating metals such as Iron, Copper, and Zirconium, provide exceptional adsorption capacities and selectivity due to tunable coordination environments and functionalized organic linkers. These properties make transition metal-based MOFs highly efficient for applications such as gas storage, catalysis, and pollutant removal (Zhang et al. 2022). Despite superior performance, transition metal-based MOFs present significant environmental concerns, including toxicity from potential metal leaching, a high environmental footprint due to energy-intensive synthesis, and complex disposal requirements. Selecting between MOFs based on alkaline earth metals and those incorporating transition metals depends on the particular requirements of the intended application, balancing the superior performance and versatility of transition metal-based MOFs against the sustainability and lower ecological impact associated with alkaline earth metal-based MOFs. By using these elements in the design and development of biocompatible MOFs, it is possible to create adsorbents that are sustainable, robust, and recyclable.

As a novel and biocompatible MOF, Ca-MOFs hold exceptional promise, especially in the domains of environmental and health protection (Table S1). While previous studies have explored the use of different metal ions in MOFs, this work outshines them by prioritizing crucial factors such as health considerations and the absence of harmful by-products. Ca-MOFs have been applied sparingly to purify water polluted with both organic and inorganic pollutants. An early Ca-MOF that has been investigated for PPCPs adsorption is the calcium-terephthalate MOF (Ca-BDC). The synthesis of this non-toxic MOF with a terephthalic acid linker was carried out for the purpose of adsorbing curcumin. Significant curcumin loading was observed in the Ca-BDC (140 mg/g) (George et al. 2019). These results imply that applications for adsorption and drug delivery could be used by Ca-MOFs. In this work, several Ca-MOFs were prepared for adsorbing emerging micropollutant such as EE2 for the first time which minimal environmental impact, and remarkable efficiency in removing contaminants, establishing a new standard of excellence in the field.

Materials and methods

Materials and chemicals

Various chemicals, including calcium carbonate ($CaCO_3$), 1,4-benzenedicarboxylic acid (H_2BDC), benzene-1,3,5-tricarboxylic acid (H_3BTC), humic acid (HA), and sodium hydroxide (NaOH) were procured from Sigma-Aldrich (USA). High-quality 17α-ethynylestradiol (EE2) standards were obtained from Dr. Ehrenstorfer (Augsburg, Germany), whereas pristine internal standards (progestrone-d9) were obtained from Toronto Research Chemicals Inc. (Ontario, Canada). To protect against photochemical degradation, a combined solution of internal and external working standards was prepared using methanol and stored at −20 °C. Milli-Q water (MQW) with water sensitivity exceeding 18.2 ΩM cm at 25 °C was purified using a Millipore system (Massachusetts, USA). Strata-X polymeric reversed-phase cartridges (C18, 200 mg/6 mL) were supplied by Phenomenex (California, USA). Fisher Scientific supplied All chemicals used in sample extraction and instrument analysis were of methanol, ethanol, acetone, acetonitrile, dimethylformamide (DMF), hydrochloric acid (HCl), high-performance liquid chromatography (HPLC), and liquid chromatography-mass spectrometry (LC–MS) grade (New Jersey, USA). The reagents were used as received without additional purification.

Synthesis of Ca-MOFs

Novel Ca-MIX was synthesized following the procedures outlined in previous studies (Sukatis et al., 2024). Ca-MIX was synthesized by dissolving H_2BDC, H_3BTC, and $CaCO_3$ in a solution consisting of equal amounts of water and DMF at molar ratios of 1:1:0.33 of each organic linker to the metal. The mixture was mixed about 15 min using a magnetic stir bar. Then, the blend was placed into stainless-steel autoclave lined with Teflon and heated in an oven at 120 °C for 16 h. The resulting solution was allowed to cool. Next, the product was filtered and washed with 20 mL DMF, water, and methanol to eliminate any impurities. The resulting material was then dried overnight in a heated oven at 100 °C to remove excess solvent prior to getting collected in a firmly sealed desiccator for further examination. Meanwhile, Ca-BDC and Ca-BTC was synthesis based on previous literature with slightly modification (Jamil et al. 2020; Sumida et al. 2016). The mixture of 1:1 M ratio of the $CaCO_3$ and H_2BDC was liquefied in 20 mL of a mixture of water and DMF for Ca-BDC, while H_3BTC was used for Ca-BTC synthesis instead of H_2BDC. The mixture was stirred thoroughly before being placed in an autoclave and heated in a 120 °C oven for 24 h. To remove impurities, the sample was collected and washed with different solvent such as DMF, water, and methanol. This methodology highlights the critical role of controlled molar ratios, solvent mixtures, and reaction conditions in achieving the desired crystallinity, porosity, and purity of the Ca-MOFs. The combination of washing and drying steps ensured the removal of impurities and stabilization of the frameworks, aligning with the optimized synthesis processes discussed in the manuscript.

Characterization

The morphology and elemental composition of the materials were analyzed using scanning electron microscopy

integrated with energy-dispersive X-ray spectroscopy (SEM–EDX), conducted with a FEI NOVA NANOSEM 230 (USA) operating at a high voltage of 30 kV. SEM images were obtained at a 10 µm scale to provide a clearer insight into the material's surface structure, allowing for clear observation of the material's structure which around 2–10 µm (Jamil et al. 2020). The surface area, total pore volume, and average pore size of the Ca-MOFs were assessed by Brunauer–Emmett–Teller (BET) analysis using a Tristar II Plus instrument (USA). The specific surface area and pore features of the samples were evaluated by examining the adsorption isotherms over a relative pressure range of 0.01 to 1.00. Nitrogen (N_2) adsorption measurements were conducted at 196 °C following a 12-h evacuation of the samples at 150 °C before adsorption. Thermal stability of synthetic materials was determined using Thermogravimetric Analysis (TGA) (USA). The percentage of weight loss was determined from thermogravimetric curves obtained under a continuous nitrogen flow of 50 mL/min, with heating conducted at a rate of 10 °C/min from 25 °C to 600 °C. Thermo Scientific Nicolet-6700 (USA) Analysis of the functional groups in the Ca-MOFs was conducted via Fourier transform infrared (FTIR) spectroscopy, with the sample subjected to scanning across the wavelength range of 400–4000/cm. An X-ray powder diffraction (PXRD) examination was executed on a PANalytical X'pert Pro PW3040 MPD X-Ray Diffractometer with Cu K radiation (0.15406 nm) in the 5° to 80° range to assess the crystallinity of the samples.

Batch adsorption

Adsorption batches were conducted in a covered volumetric flask placed on a temperature-controlled orbital shaker set at 200 rpm. The controlled temperature ensured consistent adsorption conditions by minimizing thermal fluctuations, which could influence adsorption kinetics and equilibrium. The agitation at 200 rpm facilitated uniform mixing of the Ca-MOFs and EE2 solution, preventing sedimentation and enhancing mass transfer between the adsorbent and EE2 molecules. Different amounts of Ca-MOFs, ranging from 5 to 100 mg, were introduced into 25 mL of EE2 solution at a concentration of 10 µg/L to evaluate adsorption efficiency under these controlled conditions. Batch adsorption experiments were conducted by adding different concentrations of EE2, varying from 0.1 to 200 µg/L. The effect of contact time was examined over a duration of 10 to 300 min using 50 mg of Ca-MOFs under ambient temperature conditions and a pH of 7 ± 0.5. Significant amounts of NaOH and HCl were introduced to regulate the solution's pH. The impact of ionic strength was explored by introducing a various NaCl concentration (10 to100 mg/L) into 10 µg/L EE2 solutions at pH 7 at room temperature. The effect of humic acid (HA) was evaluated by introducing different concentrations of HA (10 to 100 mg/L) into EE2 solutions (10 µg/L) under the same experimental conditions. The impact of temperature was investigated under various adsorption temperature (30, 40 and 50 ℃). To evaluate the reusability of the adsorbent, it was recovered and subjected to a regeneration process. The adsorbed EE2 was removed using a solvent treatment and then air-drying at room temperature. The regenerated material was subsequently reused in a fresh adsorption experiment. This cycle, involving adsorption, desorption, and recycle, was iterated to evaluate both effectiveness and potential shifts in performance. The samples were collected to evaluate the adsorption capacity of EE2. Prior to LC–MS/MS analysis, solid-phase extraction (SPE) was employed to enrich EE2, remove matrix interferences, and enhance detection sensitivity. The SPE process involved selective retention of EE2, allowing for its concentration while eliminating potential contaminants. This preparatory step ensured improved accuracy, precision, and reproducibility in the quantification of EE2 by facilitating optimal sample purification and solvent compatibility for LC–MS/MS analysis. To determine the adsorption capacity at equilibrium (q_e, µg/g) and the percentage of EE2 removal (R, %), Eqs. (1) and (2) were applied, which are fundamental in adsorption studies to evaluate the efficiency and capacity of the adsorbent material.

$$q_e = \frac{(C_o - C_e)V}{m}, \tag{1}$$

$$R\% = \frac{C_o - C_e}{C_o} \times 100, \tag{2}$$

where m (g) denotes the Ca-MOFs dosage, V (L) is the solution volume, C_o (µg/L) denotes the initial EE2 concentration, and C_e (µg/L) is the EE2 concentration at equilibrium. Equation (1) quantifies the amount of EE2 adsorbed per unit mass of Ca-MOFs at equilibrium, providing insight into the adsorption capacity of the material. Equation (2) determines the removal efficiency of EE2, which is a key parameter for assessing the effectiveness of the adsorption process. The accuracy of these calculations depends on several factors, including the initial EE2 concentration, adsorbent dosage, solution volume, contact time, pH, and temperature. These parameters influence the equilibrium between the adsorbate and the adsorbent, thereby affecting both adsorption capacity and removal efficiency. To ensure reliable results, experimental conditions were carefully controlled to minimize variations in these factors.

Adsorption isotherm, kinetic, and thermodynamic studies

This research employed the Langmuir, Freundlich, and Temkin adsorption isotherm models to assess the

adsorption of EE2. These models offer a means to interpret the adsorption process of EE2 on different Ca-MOFs. The Langmuir isotherm model assumes no interaction between the adsorbent and adsorbate, representing a uniform change in free energy over each of the adsorption sites. On the other hand, the Freundlich isotherm model proposes that the adsorption energy diminishes exponentially as the adsorbent nears saturation. The Temkin model assumes that adsorption happens via a uniform scattering of binding energies, culminating in a maximum binding energy. The Langmuir, Freundlich, and Temkin models are as follows:

Langmuir isotherm:

$$\frac{1}{q_e} = \frac{1}{q_m K_L} + \frac{1}{q_m} C_e. \tag{3}$$

Freundlich isotherm:

$$\ln q_e = \ln K_F + \frac{1}{n} \ln C_e. \tag{4}$$

Temkin isotherm:

$$q_e = B \ln A_T + B \ln C_e, \tag{5}$$

$$B = \frac{RT}{b_T}. \tag{6}$$

In this context, q_e (µg/g) represents the amount of EE2 that can be adsorbed by the Ca-MOFs at equilibrium, while q_m (µg/g) indicates the maximum adsorption capacity, and C_e (µg/L) refers to the EE2 concentration at equilibrium. The isotherm parameters include K_L (L/µg), which represents the Langmuir constant, K_F, associated with the sorption capacity of the Ca-MOFs, $1/n$, which indicates the strength of adsorption, T (K) denoting temperature, and R (8.314 J/mol K), the universal gas constant. B (J/mol) corresponds to the heat of sorption, b_T (J/µg) is the Temkin isotherm constant, and A_T (L/µg) denotes the Temkin equilibrium binding constant.

The study on EE2 adsorption employed both the pseudo-first-order and pseudo-second-order models as kinetics models. To gain deeper insight into EE2 adsorption and clarify the chemisorption characteristics of the equilibrium system, the Elovich kinetics model was employed. Additionally, the intraparticle diffusion model was applied to characterize adsorption kinetics by fitting the adsorption data to the intraparticle diffusion model plot. This allowed for a better understanding of the adsorption mechanism involved. The formulation of the kinetics model is depicted as follows:

Pseudo-first-order model:

$$\ln \left(q_e - q_t\right) = \ln q_e - k_1 t. \tag{7}$$

Pseudo-second-order model:

$$\frac{t}{q_t} = \frac{1}{k_2 \left(q_e\right)^2} + \frac{t}{q_e}. \tag{8}$$

Elovich model:

$$q_t = \frac{1}{b} \ln (ab) + \frac{1}{b} \ln t. \tag{9}$$

Intraparticle diffusion model:

$$q_t = k_i t^{0.5} + C. \tag{10}$$

In this context, q_t (µg/g) represents the adsorption capacity at any given time, while q_e (µg/g) signifies the adsorption capacity at equilibrium. The rate constants k_1 (1/min) and k_2 (1/min) correspond to the pseudo-first-order and pseudo-second-order adsorption rate constants, respectively. The contact time during adsorption is denoted by t (min). Additionally, α (µg/g min) refers to the initial adsorption rate, β (g/µg) is the desorption coefficient, k_i (µg/g min) indicates the rate of intraparticle diffusion, and C (µg/g) represents the intercept in the linear form of the intraparticle diffusion model.

To evaluate whether the adsorption of EE2 onto different Ca-MOFs is endothermic or exothermic, adsorption experiments were carried out at varying temperatures. The influence of temperature was examined to determine key thermodynamic parameters, including enthalpy change (ΔH°), entropy change (ΔS°), and Gibbs free energy change (ΔG°) in kJ/mol. These parameters were derived using Eqs. (11) and (12) at different temperature conditions.

$$InK_L = \frac{\Delta S^o}{R} - \frac{\Delta H^o}{RT}, \tag{11}$$

$$\Delta G^o = RTInK_L. \tag{12}$$

K_L (L/mg) denotes the Langmuir Isotherm constant at different temperatures, while R refers to the universal gas constant (8.314 J/mol-K) and T represents the absolute temperature. The values of ΔH_o and ΔS_o were obtained by analyzing the slope and intercept of the plot of ln K_L versus $1/T$.

Results and discussion

Characterization of materials

SEM images at a magnification of 10 µm confirmed the successful synthesis of Ca-MIX, revealing irregularly shaped particles with sizes predominantly below 20 µm. The morphology of the Ca-MIX samples displayed a subtle degree of homogeneity, characterized by irregularly shaped particles

and prisms with textured surfaces and varying dimensions. Microcrystals within the Ca-MIX structure measured between 5 to 10 µm, while smaller particles, attributed to residual materials, were removed during the washing process (Jamil et al. 2020; Sargazi et al. 2018). Notably, the average particle size of Ca-MIX was smaller than those of Ca-BDC and Ca-BTC, where particles exceeding 20 µm were observed. This distinction suggests that the nucleation and growth of Ca-MIX were influenced by the synergistic effect of the mixed orientations of the BDC and BTC linkers. In contrast, Ca-BDC and Ca-BTC exhibited morphologies consisting of larger, smooth square-like particles and irregular nanoparticles. The elemental composition determined through energy-dispersive X-ray (EDX) analysis (Fig. S1d–f) and corroborated by elemental analysis (Table 1) further validates the successful incorporation of calcium (Ca), carbon (C), and oxygen (O) into the Ca-MOFs. Ca-MIX displayed a higher carbon content (57.04%) compared to Ca-BDC (45.92%) and Ca-BTC (49.82%), likely due to the influence of the dual-linker system on the overall framework composition. Additionally, the significantly lower calcium content in Ca-MIX (1.92%) compared to Ca-BDC (8.34%) and Ca-BTC (5.32%) suggests differences in the coordination environment and linker interactions during synthesis. These elemental variations align with the observed differences in morphology and BET surface areas, with Ca-MIX achieving a surface area of 20.45 m^2/g and an average pore size of 12.51 nm, comparable to Ca-BTC but smaller than Ca-BDC. These findings emphasize the role of the organic linker mixture in influencing the physicochemical properties, morphology, and elemental composition of the synthesized Ca-MOFs, highlighting the unique attributes of Ca-MIX for potential applications. Differences in linker orientation and elemental composition significantly influence the nucleation, growth, and morphology of Ca-MIX compared to Ca-BDC and Ca-BTC. The dual-linker system in Ca-MIX introduces mixed orientations, creating a synergistic coordination environment that promotes heterogeneous nucleation and slower crystal growth (Dong et al. 2023). This results in smaller, irregularly shaped particles with textured surfaces and microcrystals, reflecting complex growth dynamics. In contrast, the single-linker systems in Ca-BDC and Ca-BTC provide uniform coordination environments, enabling more predictable nucleation and faster growth rates. This leads to larger, more consistent particles, with Ca-BDC forming smooth square-like structures and Ca-BTC producing irregular nanoparticles (Łuczak et al. 2023). Additionally, the higher carbon content and lower calcium coordination in Ca-MIX contribute to increased structural heterogeneity, whereas Ca-BDC and Ca-BTC exhibit denser crystal frameworks due to stronger calcium-linker interactions. These variations highlight the critical role of linker design in determining the structural and morphological properties of Ca-MOFs.

The porosity properties of each Ca-MOF were ascertained via the BET method (Garzón-Tovar et al. 2015). Table 1 shows the basic surface characterizations of Ca-BDC, Ca-BTC, and Ca-MIX. The specific surface area was 21.73, 18.55, and 20.45 m^2/g for Ca-BDC, Ca-BTC, and Ca-MIX respectively, which slightly consistent with other types of Ca-MOFs (Al-Terkawi et al. 2016; Vishnoi et al. 2016; Liao et al. 2019; Alavijeh et al. 2019). Ca-MIX had a substantially lower surface area than Ca-BDC, which might be clarified by possible coordination deficiencies around the calcium centers caused by the different connectivity of each linker, which may prevent full 3D porosity formation (Puerto-Rodríguez et al. 2022). However, surface area of Ca-MIX slightly higher than Ca-BTC which may be attributed to the fact that BDC linker could enhance the porosity of Ca-BTC. Moreover, these materials are categorized as mesoporous, with pore sizes ranging from 2 to 50 nm (Esfandiari et al. 2018). Additionally, calcium tends to create a more compact structure when combined with an organic linker, leading to lower porosity (Yang et al. 2017). Variations in the calcium coordination environment and organic linker interactions significantly influence the surface area and porosity characteristics of Ca-MOFs. In Ca-MIX, the dual-linker system leads to coordination deficiencies, resulting in a moderate BET surface area, while Ca-BDC show higher surface areas due to more uniform coordination. The BDC linker in Ca-MIX enhances porosity compared to Ca-BTC, although the mixed-linker system introduces structural heterogeneity, reducing overall porosity compared to Ca-BDC. The surface areas of the Ca-MOFs correlate with their coordination environment, with Ca-MIX balancing porosity and structural stability, Ca-BDC showing the highest surface area due to efficient coordination, and Ca-BTC having the lowest surface area, demonstrating the influence of linker

Table 1 Basic physicochemical properties of prepared Ca-MOFs

Ca-MOFs	Basic properties			Elemental analysis (%)		
	BET surface area (m^2/g)	Total pore volume (cm^3/g)	Average pore size (nm)	Ca	O	C
Ca-BDC	21.73	0.06	11.39	8.34	45.74	45.92
Ca-BTC	18.55	0.05	12.59	5.32	44.86	49.82
Ca-MIX	20.45	0.06	12.51	1.92	41.01	57.04

properties on framework formation. Figure 1a–c show the N_2 adsorption–desorption isotherms, and pore size distribution curves of Ca-BDC, Ca-BTC, and Ca-MIX. Additionally, the N_2 adsorption–desorption isotherms exhibit a reversible Type III adsorption pattern, indicating the formation of multilayers through a physisorption process, where the interaction between the adsorbate and adsorbent is stronger than the interaction between the adsorbate and the surface. There are no flat sections in the curve which monolayer formation might unavailable. This pattern indicates multilayer physisorption, where interactions between adsorbate molecules are stronger than those between the adsorbate and the adsorbent surface, suggesting limited adsorption sites with weak surface interactions. These characteristics are consistent with the mesoporous structure of Ca-MOFs, featuring pore sizes ranging from 2 to 50 nm, which support moderate adsorption capacities and reversible adsorption processes. Such properties make Ca-MOFs suitable for applications requiring dynamic adsorption–desorption cycles or controlled release systems. However, the lack of strong adsorption sites limits their applicability in processes requiring high adsorption affinity or selectivity, emphasizing the importance of understanding sorption mechanisms in tailoring material properties for specific applications. These results were consistent with the pore size distribution plots (Fig. 1c) indicated that Ca-MOFs have some micropores and mesopores structures. The findings also demonstrate that the Ca-MOFs were successfully synthesized using the solvothermal method.

Figure 1d presents the thermogravimetric analysis (TGA) curves for Ca-BDC, Ca-BTC, and Ca-MIX, illustrating their thermal stability profiles. The TGA curves reveal two main stages of weight loss for all three samples. During the initial stage, a weight reduction of about 10% is observed below 200 °C, which is attributed to the elimination of coordinated moisture and uncoordinated organic linkers, in agreement with earlier studies (Liang et al. 2011; Mallick et al. 2012; Li et al. 2018; Jamil et al. 2020). For Ca-BDC, the weight remained nearly constant with a temperature increase up to 600 °C, indicating higher thermal stability compared to the other samples. In contrast, Ca-BTC and Ca-MIX exhibited stable weight up to about 350 °C, beyond which significant weight loss was observed. The weight loss for Ca-MIX between 350 °C and 500 °C was more pronounced, with approximately 45% of its total mass lost. This substantial weight loss is likely due to the collapse of the material's framework, resulting in the formation of metal residues. The second stage of degradation begins around 600 °C for all samples, attributed to the complete breakdown of the MOF structures. This process involves the combustion of the organic linkers and the disruption of the Ca–O coordination bonds (Li et al. 2018). The residual masses at 800 °C were

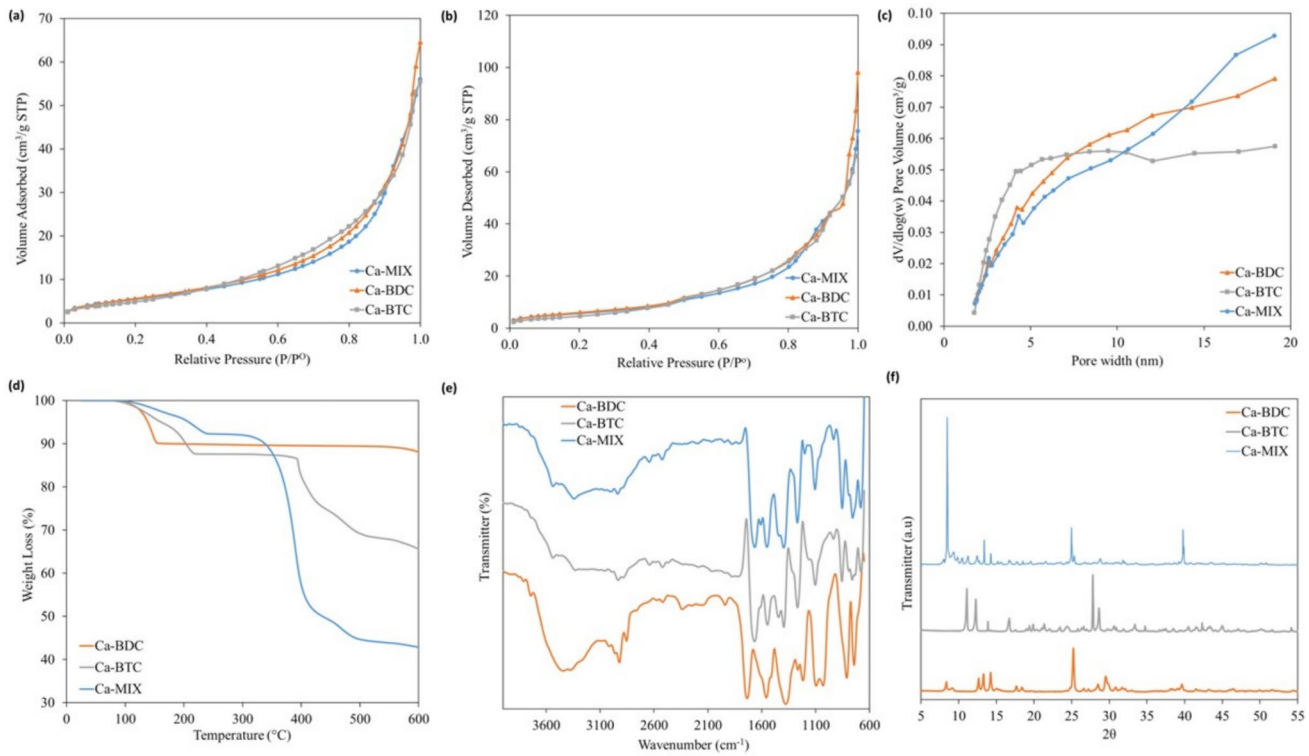

Fig. 1 **a** N_2 adsorption and **b** desorption isotherms, **c** the pore size distribution, **d** The TGA curves, **e** FTIR spectra, and **f** The XRD patters of Ca-BDC, Ca-BTC, and Ca-MIX

88.09% for Ca-BDC, 65.61% for Ca-BTC, and 42.85% for Ca-MIX, highlighting differences in thermal decomposition behavior. These results suggest that Ca-BDC exhibits superior thermal stability, whereas the mixed-linker system in Ca-MIX contributes to earlier framework degradation. The greater thermal stability of Ca-BDC and Ca-BTC compared to Ca-MIX can be attributed to their single-linker systems, which result in more uniform and robust frameworks. In contrast, the mixed-linker system in Ca-MIX introduces structural heterogeneity and potential defects, weakening the overall framework. The varied coordination of calcium ions with two distinct linkers (H_2BDC and H_3BTC) in Ca-MIX may lead to less stable metal–ligand interactions compared to the stronger and more consistent coordination environments in Ca-BDC and Ca-BTC. Additionally, the irregular pore structure in Ca-MIX likely reduces its mechanical integrity, making it more susceptible to thermal decomposition. These factors collectively contribute to the superior thermal stability observed in Ca-BDC and Ca-BTC. Thermal stability is a critical property for potential applications, particularly in environmental remediation, where materials may be exposed to varying temperatures during adsorption, desorption, or regeneration processes. Furthermore, understanding the thermal decomposition behavior provides insights into the robustness of the Ca-MOFs and their potential durability under operational conditions.

The FTIR spectra of the Ca-MOFs nanocomposite are presented in Fig. 1e. Distinct peaks between 3500 cm^{-1} and 3300 cm^{-1} are observed, which correspond to O–H stretching vibrations, indicating the presence of functional groups such as phenols and carboxylic acids in all the Ca-MOFs (Kojima et al. 2018; Nguyen et al. 2019). Furthermore, peaks at 1267, 1198, and 1103 cm^{-1} suggest O–H bending due to hydrogen bonding with water molecules and Ca-O interactions. A peak around 1664 cm^{-1} is attributed to an O-C-O stretch, likely associated with ionic carbonyl linkages forming a bidentate bridge (Shi et al. 2010; George et al. 2019; Sun et al. 2019). Peaks between 930 and 850 cm^{-1} confirm the presence of Ca-O stretching, indicating the formation of Ca-MOFs through the calcium-oxo group (George et al. 2019). Finally, peaks in the range of 750 to 680 cm^{-1} are assigned to C-H bending vibrations in the benzene ring.

Figure 1f shows the PXRD spectra of the Ca-BDC, Ca-BTC, and Ca-MIX, respectively. The Ca-MOFs samples of Ca-BDC, Ca-BTC, and Ca-MIX are generally shown a crystallite structure. When comparing the PXRD patterns of Ca-MIX to Ca-BDC and Ca-BTC, there was a noticeable difference in the scattering peaks, indicating the presence of different and additional phases (Puerto-Rodríguez et al. 2022). In contrast to the FTIR findings, it's noticeable that each sample displays a unique phase pattern, suggesting identical chemical compositions but varying atomic arrangements. PXRD pattern for Ca-MIX shown some intense peaks showed that Ca-MIX exhibit with great crystallinity properties than Ca-BDC and Ca-BTC. Therefore, it could be resolved that variations in the carboxylate linkers would have an effect on the structure of Ca-MOFs differently dependent on their symmetry. The nucleation process of Ca-MIX is governed by the coordination interactions between calcium ions (Ca^{2+}) and the organic linkers, which dictate the crystallization pathway and structural formation. BTC, with its three carboxylate groups, exhibits a higher coordination affinity with Ca^{2+}, leading to faster nucleation and the formation of a densely cross-linked structure (Liang et al. 2011). In contrast, BDC, possessing two carboxylate groups, facilitates slower nucleation, allowing for controlled crystal growth and a more open framework (George et al. 2019). The combination of both linkers in Ca-MIX creates a synergistic effect, balancing nucleation rates and promoting the formation of a well-defined crystalline structure with controlled porosity (Ramzan et al. 2023). The structural influence of BTC and BDC linkers in the formation of Ca-MIX is evident in their differing effects on morphology. BTC enhances framework compactness due to its higher coordination affinity, while BDC increases flexibility, altering the overall structure (Roslan et al. 2024). XRD analysis confirms these structural variations by revealing differences in crystallinity and phase composition within the mixed-linker system. Additionally, the SEM images depict morphological distinctions, emphasizing the role of linker selection in crystal growth and surface characteristics (Carpenter et al. 2023) (Han et al. 2022) (Łuczak et al. 2023).

These results, in combination, provided a robust framework for evaluating the structural, chemical, and thermal properties of synthesized Ca-MOFs. The integration of SEM–EDX, BET, FTIR, PXRD, and TGA ensured a thorough understanding of the material's characteristics, enabling optimization of synthesis methods, and enhancing the applicability of Ca-MOFs in contaminant removal.

Effects of Ca-MOFs dosage

The interaction between adsorbent binding sites and EDCs is influenced by multiple parameters, including adsorbent dosage, initial EE2 concentration, and solution volume, all of which impact the adsorption rate (Liu et al. 2019). The relationship between adsorption capacity and Ca-MOFs dosage demonstrates that EE2 adsorption capacity decreases significantly as the Ca-MOFs mass increases from 5 to 25 mg ($p < 0.05$) (Fig. 2). This trend suggests that, despite an increase in available adsorption sites with higher Ca-MOF dosages, the actual uptake of EE2 per unit mass of adsorbent declines.

At low Ca-MOF dosages (5–25 mg), adsorption efficiency increases due to a greater availability of sorption sites. A higher number of binding sites facilitates stronger

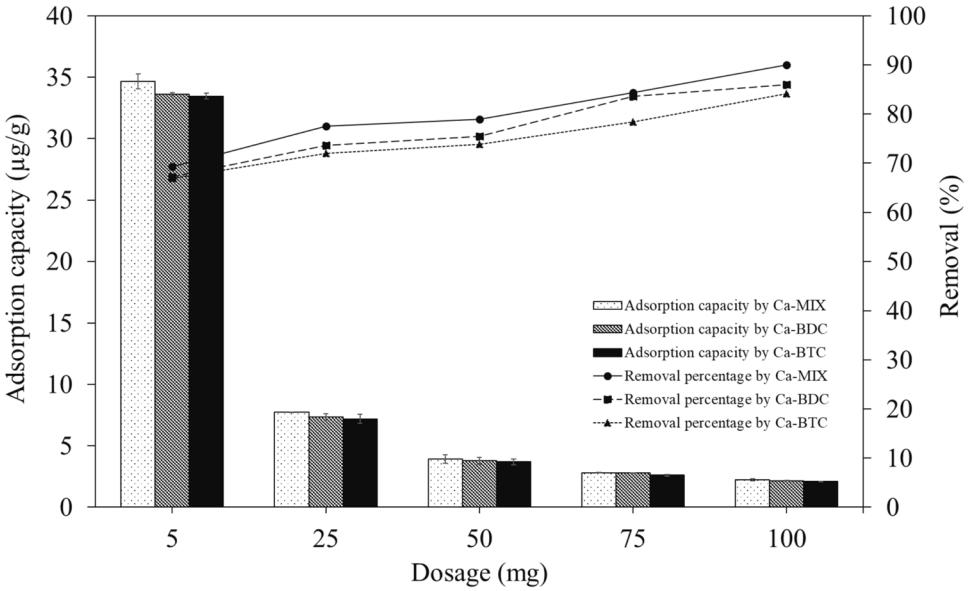

Fig. 2 Effect of different adsorbent dosage (initial concentration: 10 μg/L; contact time: 4 h; pH: initial state)

interactions between EE2 molecules and Ca-MOFs, promoting rapid adsorption (Rezania et al. 2021; Adegoke et al. 2022). The high surface-to-volume ratio at lower adsorbent doses allows EE2 to effectively diffuse into and bind with the Ca-MOFs. Beyond 25 mg, a decrease in EE2 adsorption capacity per gram of Ca-MOFs is observed, which can be attributed to particle agglomeration at higher adsorbent concentrations. When Ca-MOFs are present in excess, strong interparticle interactions lead to aggregation, reducing the overall surface area available for EE2 binding. Furthermore, longer diffusion path lengths are introduced, making it more difficult for EE2 molecules to penetrate the inner pores of Ca-MOFs. This effect diminishes adsorption efficiency despite the increase in adsorbent quantity. Increasing the Ca-MOF dosage beyond 50 mg does not lead to a significant increase in EE2 removal efficiency, as the system approaches adsorption equilibrium. The number of EE2 molecules available in solution becomes a limiting factor, and additional Ca-MOFs do not contribute to further EE2 uptake. The formation of saturated adsorption sites prevents further adsorption, thereby stabilizing the adsorption capacity.

In evaluating the adsorption capacities of the different Ca-MOFs, Ca-MIX exhibited the highest EE2 adsorption capacity, outperforming Ca-BDC and Ca-BTC. This enhanced performance is primarily due to the higher surface area and optimal pore structure of Ca-MIX. Although Ca-BDC has a slightly larger total surface area, the average pore width of Ca-MIX is 12.16% greater than that of Ca-BDC, which improves EE2 diffusion and adsorption efficiency. As a result, Ca-MIX provides a balance between surface area and pore accessibility, making it the most effective adsorbent among the tested materials. Based on experimental results, 50 mg of Ca-MOFs was identified as the optimal adsorbent dosage, achieving the highest EE2 removal efficiency with minimal adsorbent wastage. This dosage ensures maximum EE2 uptake while preventing excessive material use, thus optimizing the adsorption process.

Kinetics studies and effect of contact time

The effect of contact time on EE2 adsorption at 10 μg/L by Ca-MOFs was investigated (Fig. 3a). The experiments revealed that adsorption increases rapidly up to 64%, 56%, and 42% in the first two hours for Ca-MIX, Ca-BDC, and Ca-BTC, respectively. Then decreases until it reaches adsorption equilibrium at 240 min. The quantity of active sites present on the adsorbents is related to this phenomenon (Hasan et al. 2013). The initial fast adsorption rates are primarily as a result of the abundance of active sites on the adsorbent's surface. As the active sites became filled, the remaining unoccupied sites on the Ca-MOFs became saturated with increasing contact time, leading to a gradual slowdown in adsorption, which eventually reached equilibrium after approximately 2 h.

To examine the operating mechanism of adsorption processes, including mass transfer and chemical reactions, an appropriate kinetic model is necessary. To better understand the adsorption kinetics of EE2, both the pseudo-first-order and pseudo-second-order models were applied to describe the adsorption behavior. As shown in Table S2, the adsorption of EE2 onto Ca-MIX, Ca-BDC, and Ca-BTC closely follows the pseudo-second-order kinetic model, with correlation coefficients (R^2) approaching unity for all three materials. Conversely, the pseudo-first-order model yielded lower correlation coefficients and rate constants, indicating its inadequacy in accurately representing the adsorption

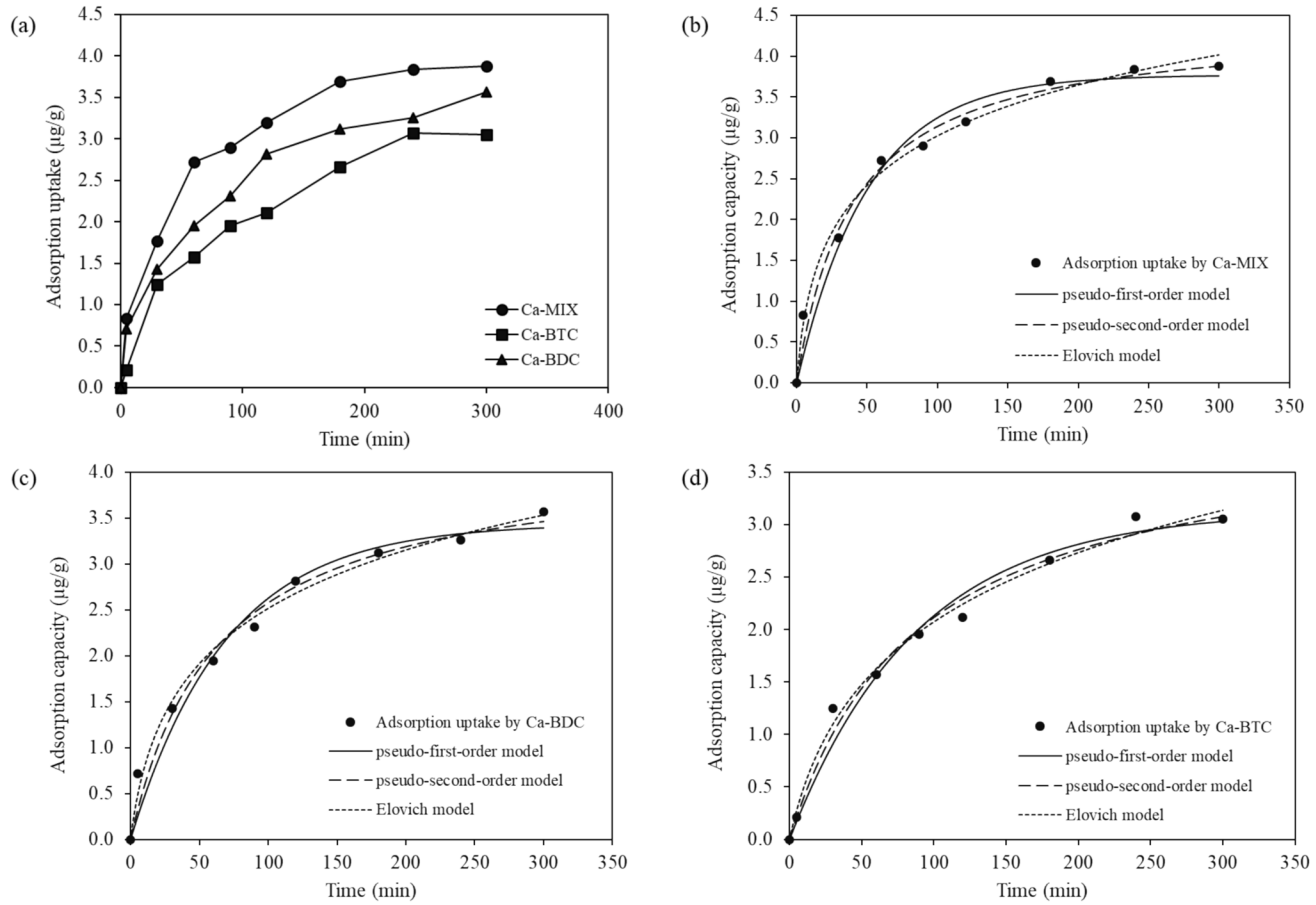

Fig. 3 **a** Effect of different contact time on the adsorption of EE2 at concentration of 10 µg/L and different non-linear kinetic adsorption models by **b** Ca-MIX; **c** Ca-BDC; and **d** Ca-BTC (initial concentration: 10 µg/L; dosage: 50 mg; pH: initial state)

behavior. The strong agreement with the pseudo-second-order model implies that the adsorption kinetics are primarily driven by chemisorption, which involves the formation of chemical bonds via electron sharing or exchange between the Ca-MOFs and ionized EE2 molecules. This mechanism highlights that the adsorption is influenced not only by the availability of active sites but also by the interactions between functional groups on the adsorbent and the adsorbate. For instance, the calcium ions and organic linkers in the MOFs provide active sites that can form bonds with EE2 molecules, contributing to the high adsorption capacity and favorable kinetics observed. These findings are consistent with prior studies that report pseudo-second-order kinetics as a characteristic of systems involving strong chemical interactions (Robati 2013; Qu et al. 2009). Moreover, adsorption behaviour that is consistent with the characteristics of chemical adsorption was described using the Elovich model. It was found that Elovich model is superior for the explanation of kinetics data for adsorption kinetics of EE2 onto Ca-MIX and Ca-BTC since the R^2 is 0.992 which slightly higher as compared to the Ca-BDC. This is probably caused by some variations in the chemical characteristics of trimesic based linker MOFs since their organic linker, H_3BTC contains a hydrogen donor and acceptor more than in Ca-BDC (H_2BDC as linker). High hydrogen donor and acceptor number might contribute to the high correlation coefficient of Elovich isotherm model for Ca-BTC and Ca-MIX as compared to the Ca-BDC, since Elovich model are typically used to elucidate the chemisorption phenomenon in adsorption process.

Based on the kinetics fitting of EE2 adsorption to the intraparticle diffusion model (Fig. S2) suggested a two-stage segment of the entire adsorption process. The adsorption rate was determined from the slope of each linear segment in the plot which a sharper slope denotes a faster adsorption process (Bhaumik et al. 2016). In the initial phase, q_t rose swiftly over time due to the fast external diffusion of EE2 onto Ca-MIX, Ca-BDC, and Ca-BTC, respectively. The second segment served as a representation of the intraparticle diffusion effect. Ca-MIX and Ca-BDC samples show higher ability of adsorption as the coefficients of correlation for this model close to one than Ca-BTC most likely owing

to their higher surface areas which allows the diffusion of EE2 molecules through the pores of the materials more easily. The schematic dimensions of the predicted intraparticle diffusion of EE2 molecule through different Ca-MOFs are shown in Fig. S3.

Isotherm studies and effect of initial concentration of EE2

The relationships of concentration of EE2 and adsorption capacity of Ca-MIX, Ca-BDC, and Ca-BTC are shown in Fig. 4. The removal rate improved as the adsorbate concentration increased, aligning with the results observed in earlier optimal dosage evaluations (Fig. 2) (Jun et al. 2019). The EE2 adsorption data showed that the adsorption capacity by all three Ca-MOFs increases as the EE2 concentration increases. For Ca-MIX, the adsorption equilibrium adsorption capacity of EE2 reached to 52.03 µg/g while the EE2 initial concentration was 200.00 µg/L, while the equilibrium uptake rates by other two Ca-MOFs were only 35.69 µg/g (Ca-BDC) and 19.49 µg/g (Ca-BTC), respectively. It was evident that the efficiency of EE2 adsorption significantly increased with rising EE2 concentrations; however, the adsorption rate eventually declined, likely due to the limited availability of active sites on the surface of the Ca-MOFs as the adsorption process approached saturation.

To have better understanding regarding the adsorption of EE2 by Ca-MOFs, the possible mechanism was studied and evaluated the adsorption equilibrium using a standard isotherm model for instance Langmuir, Freundlich and Temkin models. The Langmuir model assumes monolayer adsorption onto a homogeneous surface with a finite number of identical sites. In contrast, the Freundlich model describes multilayer adsorption on a heterogeneous surface, where adsorption sites have varying affinities. The Temkin model considers the interactions between adsorbate and adsorbent, assuming that the heat of adsorption decreases linearly with surface coverage. Table S3 shows the isotherm models parameters and correlation coefficient values for three models that could be correlated with EE2 adsorption. The adsorption

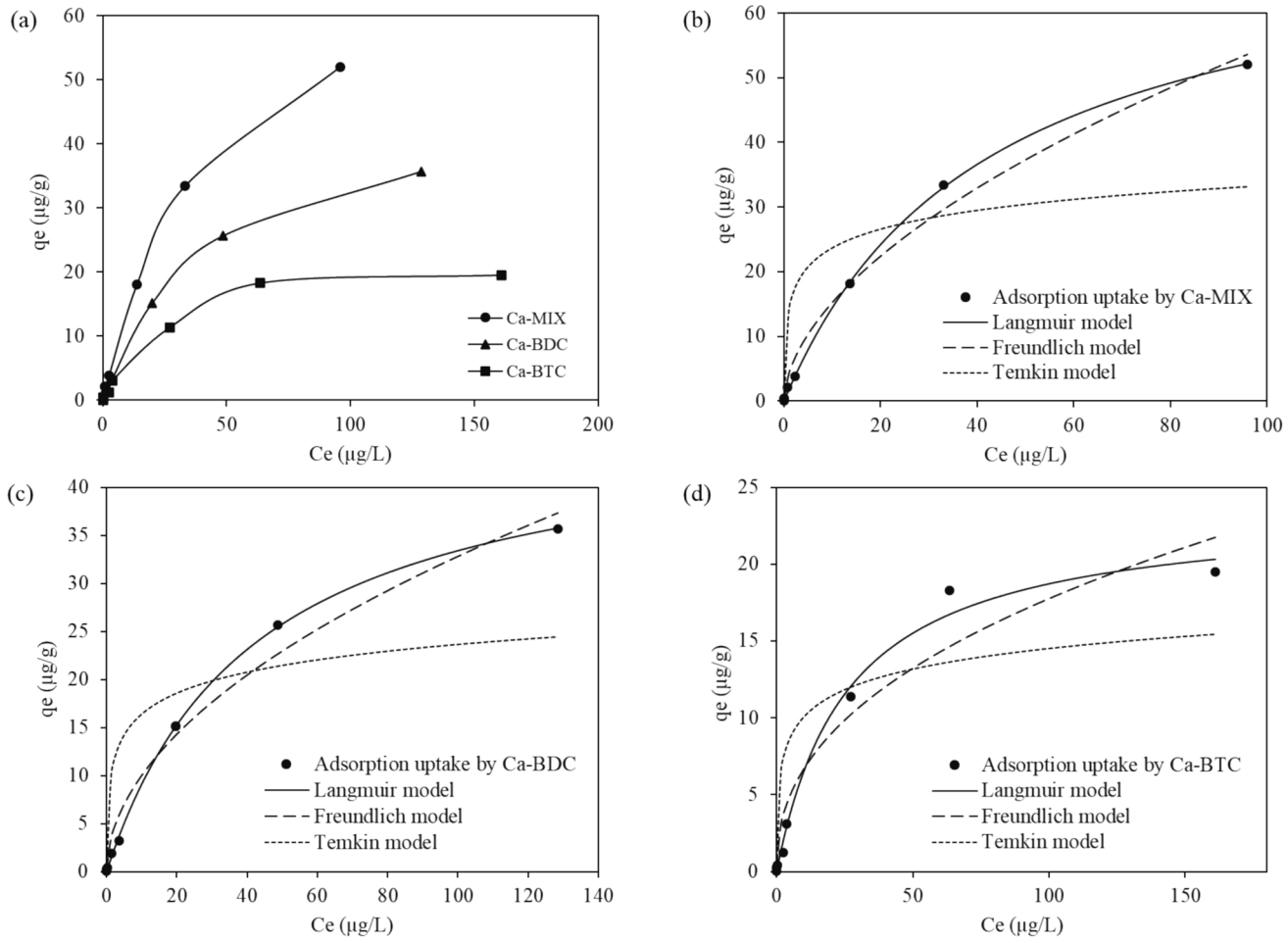

Fig. 4 Adsorption uptake of EE2 by different Ca-MOFs with **a** different initial concentration; adsorption isotherm model fitting for **b** Ca-MIX; **c** Ca-BDC; and **d** Ca-BTC (contact time: 2 h; dosage: 50 mg; pH: initial state)

mechanisms of EE2 onto Ca-MOFs (Ca-MIX, Ca-BDC, and Ca-BTC) were analysed using Langmuir, Freundlich, and Temkin isotherm models, providing insights into the interaction mechanisms. The Langmuir model, with high R^2 values for Ca-MIX and Ca-BDC (0.99), indicates strong monolayer adsorption on homogeneous surface sites, suggesting uniform interaction mechanisms. Ca-MIX demonstrated the highest adsorption capacity (q_{max} = 74.93 µg/g), reflecting its efficient interaction with EE2 molecules. The Freundlich model, which describes multilayer adsorption and surface heterogeneity, highlights that Ca-MIX (K_F = 4.22 (µg/g) (L/µg)$^{1/n}$) provides more diverse interaction sites than Ca-BDC (3.054 (µg/g) (L/µg)$^{1/n}$) and Ca-BTC (2.50 (µg/g) (L/µg)$^{1/n}$), though it fits less effectively for Ca-BTC (R^2 = 0.94).

The Temkin isotherm model provides a unique perspective on the adsorption process by incorporating the effects of indirect adsorbate–adsorbent interactions, assuming that the heat of adsorption decreases linearly with increasing surface coverage. This contrasts with the Langmuir model, which assumes uniform adsorption energy across a homogenous surface with no interactions between adsorbed molecules, and the Freundlich model, which empirically accounts for surface heterogeneity but does not explicitly consider variations in adsorption energy (Foo and Hameed 2010). In the present study, the Temkin binding energy constant (b_T) was used to evaluate the intensity of interaction between EE2 molecules and the Ca-MOFs. Among the three adsorbents, Ca-BTC exhibited the highest b_T value (1280.70 J/µg), indicating the strongest interaction energy, despite having the lowest adsorption capacity (q_{max} = 23.59 µg/g). This suggests that while Ca-BTC offers fewer adsorption sites, the energy associated with EE2 binding at those sites is significantly higher, likely due to stronger chemisorptive interactions or specific binding affinity (Zhou et al. 2022). In contrast, Ca-MIX demonstrated a more moderate b_T value (593.28 J/µg) but achieved the highest adsorption capacity (q_{max} = 74.94 µg/g), reflecting a balance between interaction strength and the availability of active sites. Additionally, Temkin's A_T values, representing the equilibrium binding constants, further suggest that Ca-MIX possesses a more favorable adsorption potential (A_T = 29.18 L/µg) compared to Ca-BTC and Ca-BDC. While the R^2 for the Temkin model were generally lower (0.647–0.730) than those of the Langmuir and Freundlich models, the model still provides valuable insights into the adsorption energy distribution, which neither Langmuir nor Freundlich explicitly capture (Chu 2021). Thus, the Temkin model highlights that although Ca-BTC exhibits stronger adsorption energy, this does not necessarily translate to higher capacity. Instead, Ca-MIX achieves superior performance by optimizing both energy interactions and surface availability, confirming that the adsorption mechanism is not solely dependent on energetic strength but also on the accessibility and heterogeneity of binding sites, as also supported by Langmuir and Freundlich model fits.

In summary, the comparative analysis of isotherm models reveals that Ca-MIX achieves optimal performance due to a synergy of uniform adsorption (Langmuir), moderate surface heterogeneity (Freundlich), and favorable interaction energy (Temkin). These results affirm that the EE2 adsorption process on Ca-MIX is predominantly monolayer and chemisorptive in nature, consistent with the findings from the kinetic studies. Three factors can be used to summarize the reasons for the different adsorption behaviour of EE2 against the three Ca-MOFs. Firstly, the Ca-MIX has a high average pore width as compared to Ca-BDC and Ca-BTC due to the mixed-linker presence might enhance porous structure of than in single-linker Ca-MOFs. Secondly, electrostatic interaction between Ca-MOFs and EE2 may perhaps effects on the adsorption trend of different point zero charge (PZC) on surface of Ca-MOFs which later would be discussed on the effect of pH of solution. Final possible reasons are due to high Log K_{OW} value of EE2, hydrophobic interaction between EE2 and Ca-MOFs might explain this adsorption performance as lead to the rapid and spontaneous adsorption nature which would be discussed on thermodynamic study.

Thermodynamics studies and effect of temperature

The influence of temperature on the adsorption of each EDC at a concentration of 10 µg/L was examined using three separate solutions across a temperature range of 30 to 50 °C. As shown in Fig. S4, the adsorption of EE2 by Ca-MOFs increased noticeably as temperature rise from 30 to 50 ℃, suggesting that this adsorption is endothermic in nature. At 50 ℃, the extent of adsorption EE2 by Ca-MIX was nearly 90%, while 86% and 82% for Ca-BDC and Ca-BTC, respectively. The effects of an increase in solution temperature having a clear impact on adsorption due to an increased diffusion rate are the main reason of this phenomenon, indicating that solution temperature has a substantial impact on adsorption (Qu et al. 2009). It was discovered that 50 °C was the ideal temperature for the adsorption, which corresponds to a high adsorption capacity.

The observed increase in adsorption with rising temperature can be attributed to an enhanced diffusion rate of EE2 molecules in the solution, which facilitates better interaction between the adsorbate and the adsorbent surface. This phenomenon aligns with the theory that higher temperatures can increase molecular motion, thereby improving the mass transfer rate and making adsorption sites more accessible (Prokić et al. 2022; Kul et al. 2023). As the temperature increased from 30 °C to 50 °C (Fig. S4), the adsorption capacity of Ca-MIX increased from 3.67 µg/g to 4.47 µg/g, Ca-BDC from 3.63 µg/g to 4.32 µg/g, and Ca-BTC from

3.37 µg/g to 4.14 µg/g, indicating that higher temperatures favor more efficient adsorption.

The thermodynamic parameters for the EE2 adsorption towards various Ca-MOFs are summarized in Table S4. The results exhibited that temperature is a substantial additional factor that can influence EE2 adsorption by Ca-MOFs. The value of enthalpy change, ΔH° obtained here are + 45.117, + 35.268, and + 33.859 kJ/mol for Ca-MIX, Ca-BDC, and Ca-BTC, respectively. The positive enthalpy change signifies that the adsorption process absorbs heat, indicating its endothermic nature. Additionally, the negative Gibbs free energy change ($\Delta G°$) at all temperatures suggests that the adsorption of EE2 onto each Ca-MOF occurs rapidly and spontaneously. A positive value of entropy, ΔS°, is correlated with a rise in the degree of freedom of the adsorbed compounds. Additionally, the positive ΔS° value suggests that during the adsorption process, some changes take place in the internal structure of metal-frameworks.

Effects of initial pH, ionic strength, and humic acids

The effect of solution pH on EE2 adsorption is critical, as it influences the surface charge of the adsorbent, the speciation of the adsorbate, and the dominant interaction mechanisms. In this study, the pH range of 3 to 11 was selected to reflect acidic, neutral, and alkaline conditions, respectively, and was adjusted using NaOH and HCl. As shown in Fig. 5a, the adsorption capacities of Ca-MOFs varied notably with pH. The optimal adsorption capacities for EE2 were observed at pH 7 for Ca-MIX, pH 9 for Ca-BDC, and pH 5 for Ca-BTC, demonstrating that pH plays a significant role in modulating adsorption performance.

The variation in adsorption efficiency can be attributed to the changes in electrostatic interactions and hydrogen bonding, which are directly influenced by both the ionization state of EE2 and the surface charge of the Ca-MOFs. EE2 has a pKa value of 10.4 (Jun et al. 2019), indicating that it predominantly exists in a neutral molecular form under pH < 10.4, and begins to ionize into anionic species at pH > 10.4. The point of zero charge (PZC) of the MOFs, determined experimentally (Fig. 5b), was approximately 5.0 for Ca-MIX, 8.5 for Ca-BDC, and 3.5 for Ca-BTC. When the solution pH exceeds the PZC of a given MOF, its surface becomes negatively charged, which can lead to electrostatic repulsion with ionized EE2 molecules, thereby reducing adsorption efficiency. This effect is particularly evident at higher pH levels (above 9), where a marked decline in adsorption was observed for all three MOFs. Conversely,

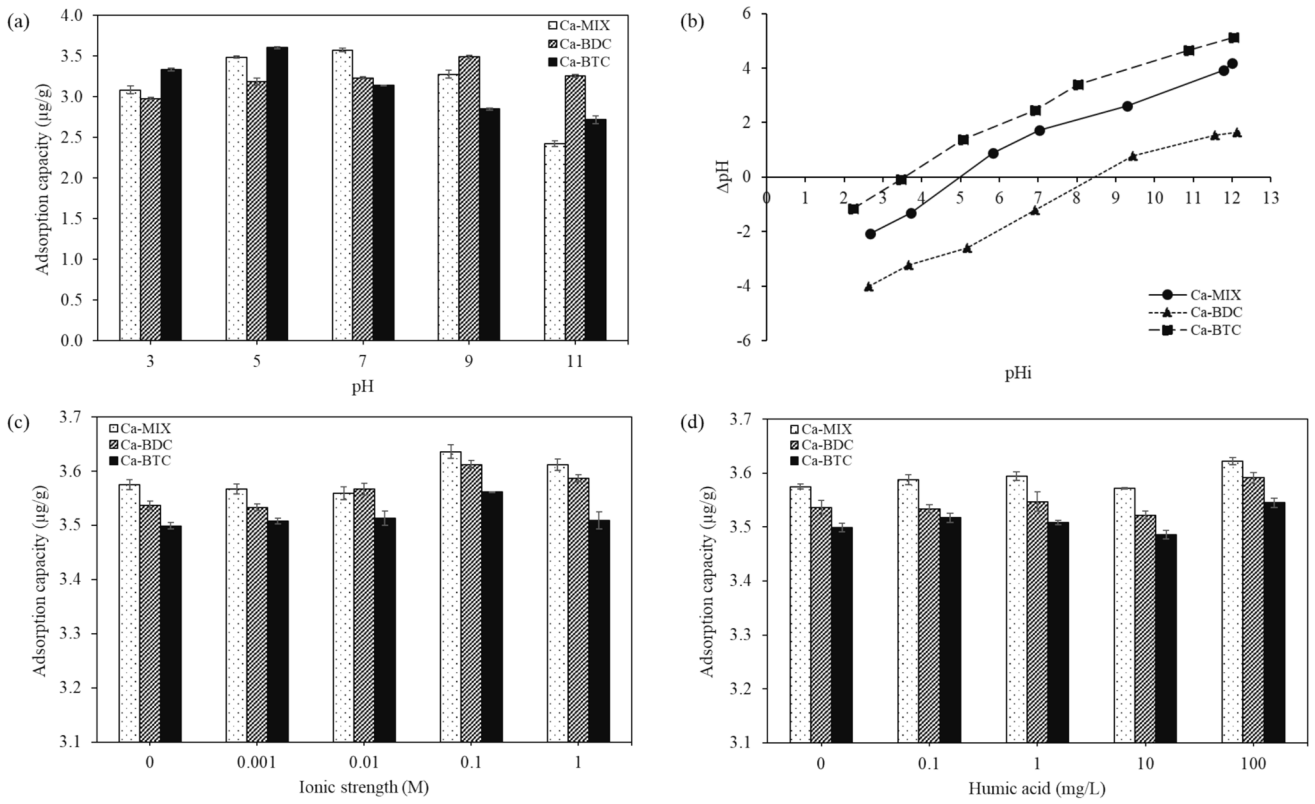

Fig. 5 **a** Effect of initial pH; **b** determination of the point of zero charge of three Ca-MOFs; **c** effect of ionic strength; and **d** effect of humic acid (initial concentration: 10 µg/L; contact time: 2 h; dosage: 50 mg; pH: initial state for humic acid and ionic strength effects)

under acidic conditions, the MOF surfaces are positively charged (pH < PZC), and EE2 exists primarily in its neutral form. This environment facilitates favorable interactions through hydrogen bonding between the electron-rich functional groups (e.g., –OH, –COOH) present on the MOF surfaces and the hydroxyl groups of EE2 (He et al. 2016; Tian et al. 2018). For instance, Ca-BTC, with a low PZC of 3.5, exhibited maximum adsorption at pH 5 due to stronger hydrogen bonding and possible π–π interactions under mildly acidic conditions. Overall, these results highlight that pH adjustment via NaOH and HCl is not merely a procedural step, but a critical factor for optimizing EE2 adsorption by controlling the balance between electrostatic interactions and hydrogen bonding. The specific pH-dependent performance of each Ca-MOF underscores the importance of tailoring operational conditions based on the physicochemical properties of both the adsorbent and the target contaminant.

The effect of ionic strength on EE2 adsorption is shown in Fig. 5c. For ionic strengths below 0.01 M, the adsorption of EE2 onto Ca-MIX and Ca-BTC remained relatively unaffected ($p > 0.05$), while Ca-BDC exhibited a slight increase in adsorption capacity. However, at ionic strengths of 0.1 M or higher, all three Ca-MOFs showed a significant increase in adsorption capacity due to the salting-out effect. This phenomenon occurs as increasing ionic strength enhances the hydrophobicity of EE2, reducing its solubility and promoting adsorption onto the Ca-MOF surfaces (Somporn-pailin et al. 2021; Yin et al. 2019). At higher ionic strength (approximately 1.0 M), a slight decline in adsorption capacity was observed. This reduction is attributed to the diminishing salting-out effect and the emergence of a squeezing-out effect. At this stage, ions infiltrate the diffuse double layer surrounding the adsorbent, reducing repulsive interactions and promoting dense aggregation of adsorbates on the adsorbent surface. Additionally, increased ionic strength promotes the ionization of the hydroxyl groups on the Ca-MOF surfaces (e.g., Ca-OH to Ca-O-), reducing their ability to participate in hydrogen bonding. This ionization also enhances electrostatic repulsion between EE2 and the negatively charged adsorbent, further contributing to the reduction in adsorption performance at high salt concentrations.

Humic acids are natural substances that form as organic matter degrades in low-oxygen environments. At neutral pH, the carboxylic substituent deprotonation gives humic acid a negative surface charge. This chemical can be found in groundwater, surface water, and soil (Jun et al. 2019; Yin et al. 2019). The influence of humic acid (HA) on EE2 adsorption by Ca-MOFs was investigated across a concentration range of 0 to 100 mg/L, representing environmentally relevant levels of dissolved organic matter. As illustrated in Fig. 5d, humic acid exhibited a concentration-dependent effect on the adsorption behavior. At low HA concentrations (≤ 1 mg/L), the adsorption capacities of EE2 on Ca-MIX, Ca-BDC, and Ca-BTC remained relatively stable and showed no statistically significant change ($p > 0.05$), with adsorption capacities ranging between 3.54–3.59 µg/g for Ca-MIX, 3.53–3.55 µg/g for Ca-BDC, and 3.50–3.51 µg/g for Ca-BTC. This suggests minimal interference by HA at trace levels. However, at 10 mg/L HA, a noticeable decrease in EE2 adsorption was observed for all three adsorbents. The adsorption capacity of Ca-MIX dropped from 3.59 µg/g to 3.44 µg/g, Ca-BDC from 3.55 µg/g to 3.47 µg/g, and Ca-BTC from 3.51 µg/g to 3.43 µg/g. This reduction is attributed to direct competition between HA and EE2 molecules for available active sites on the MOF surfaces. The negatively charged HA molecules at neutral pH, due to deprotonated carboxylic groups, are likely to compete with EE2 for adsorption through surface coverage or site-blocking effects (Newcombe et al. 2002; Yin et al. 2019).

Interestingly, at 100 mg/L HA, a reversal in trend was observed. All three Ca-MOFs exhibited increased EE2 adsorption compared to the 10 mg/L condition. The adsorption capacities increased to 3.74 µg/g for Ca-MIX, 3.64 µg/g for Ca-BDC, and 3.69 µg/g for Ca-BTC. This unexpected enhancement can be explained by the complex structural and chemical nature of HA. The presence of aromatic, non-phenolic, and hydrophobic domains within HA molecules may facilitate hydrophobic interactions with EE2, effectively forming EE2–HA complexes that enhance the proximity and retention of EE2 near or on the MOF surface (Jun et al. 2019). Furthermore, humic acids may modify the adsorbent surface chemistry, introducing new functional groups or altering surface energy, thus promoting secondary interactions such as π–π stacking, hydrogen bonding, and van der Waals forces (He et al. 2016; Zhang et al., 2022). Overall, these findings highlight that while moderate HA concentrations may hinder EE2 adsorption via competition, higher HA levels can promote adsorption through hydrophobic enhancement and surface modification effects.

Reusability of Ca-MOFs

Reusable adsorbents are crucial to the practicality and commercial viability of large-scale applications (Gkika et al. 2022). For a material to be used as an adsorbent in the actual world, it must have two crucial qualities that should be evaluated such as reusability of materials. In this study, prior to evaluating the reusability of Ca-MIX, Ca-BDC, and Ca-BTC, the spent Ca-MOFs were rinsed with three distinct solvents: methanol, ethanol, and water. Figure 6a demonstrates

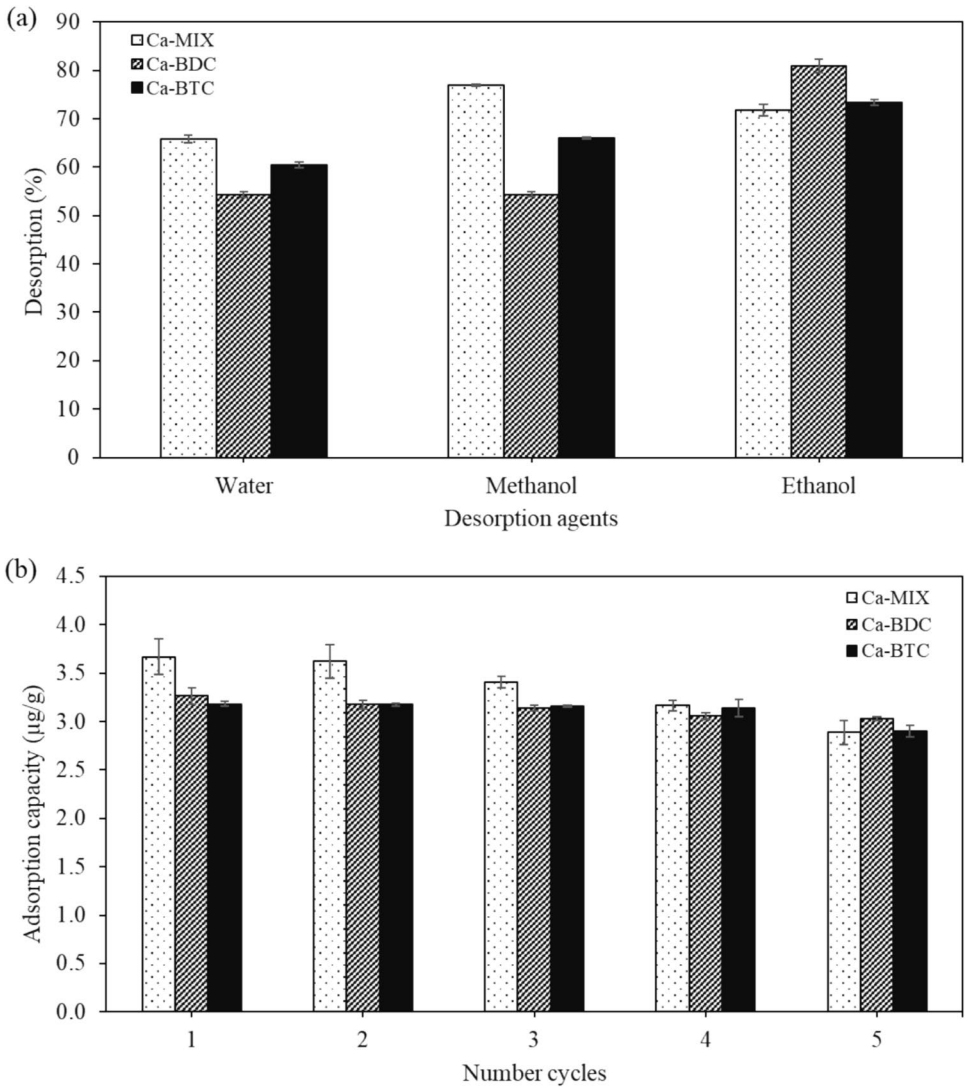

Fig. 6 **a** Desorption of EE2 using different elution agents; and **b** reusability of different Ca-MOFs for targeted EE2 removal (initial concentration: 10 μg/L; contact time: 2 h; dosage: 50 mg; pH: initial state)

that regeneration using ethanol shows an obvious advantages reusability as compared to methanol and water, respectively. This may be because of EE2 are more soluble in ethanol than in other solvents, which may account for their higher solubility in ethanol (Hasan et al. 2013). Among the tested solvents, ethanol exhibits lower polarity than methanol and water; therefore, it was chosen as the desorption medium for the regeneration process. Generally, EE2 was desorbed more effectively in ethanol, with the order of desorption being Ca-BDC > Ca-BTC > Ca-MIX. This difference in desorption efficiency can be attributed to the higher activation energy of Ca-MIX compared to Ca-BDC and Ca-BTC (Table S4) (Artioli 2008), which results in a lower amount of EE2 being desorbed from the Ca-MIX adsorbent. Despite the enthalpy value for Ca-BDC being higher than that for Ca-BTC, the desorption rate for Ca-BDC remained superior, likely due to its larger surface area, which is 17% greater than that of Ca-BTC. This larger surface area may provide more available adsorption sites, facilitating a faster desorption process. On the other hand, Ca-MIX demonstrates strong adsorption capacity due to a combination of mechanisms, including hydrophobic interactions, hydrogen bonding, and π-π interactions. These strong interactions require higher energy for desorption, which reduces its recovery efficiency during regeneration cycles. Additionally, the mixed-linker structure of Ca-MIX may introduce a variety of adsorption sites with different binding strengths, some of which may trap EE2 irreversibly, further diminishing its recoverability.

Five cycles of adsorption were used to measure the adsorption capacity (Fig. 6b). For Ca-MIX, the adsorption

performance of EE2 remained relatively consistent ($p > 0.05$) up to the fourth regeneration; nevertheless, there was a little reduction in removal rate. However, the adsorption capacity of EE2 by Ca-BDC and Ca-BTC was maintained up to fifth cycles. The adsorption capacity of EE2 by Ca-BDC, Ca-BTC, and Ca-MIX decreased slightly with increasing adsorption and desorption cycle times, with 7%, 9%, and 21% loss after five circles. The inadequate adsorbent recovery during the filtration process may be the cause of these loss percentage of Ca-MIX. Meanwhile, Ca-BDC and Ca-BTC maintained its excellent performance following regeneration, denoting that it might potentially be used as an inexpensive and efficient adsorbent for the adsorption of EE2 from water. This reusability performance could be related stability of Ca-MIX is lower than to other Ca-MOFs. As can be seen in thermal stability performance (Fig. 1d) indicated that coordination bond between calcium and organic linker in Ca-MIX is low reflecting that slightly low reusability of this MOFs. However, Ca-MIX demonstrated a higher EE2 removal capacity compared to the other two Ca-MOFs up until fourth cycles indicted that structure stability drawbacks the Ca-MIX performance. The effectiveness of Ca-MOFs in multiple cycles of adsorption and desorption is influenced by several factors, including the availability of adsorption sites, the strength of the adsorption mechanisms (such as hydrophobic interactions, hydrogen bonding, and π-π interactions), and the efficiency of the desorption process. Materials with stronger binding mechanisms, like Ca-MIX, may show reduced desorption efficiency and lower recovery due to the higher energy required for regeneration. Additionally, the stability of the material during repeated cycles is critical, as the mixed-linker structure of Ca-MIX could degrade over time, affecting long-term performance. Optimizing desorption conditions and exploring surface modifications could improve recovery and enhance the practicality of Ca-MOFs for wastewater treatment applications.

Conclusion

The removal of the synthetic estrogen; EE2 from an aqueous solution by different linker-based Ca-MOFs (i.e., Ca-MIX, Ca-BDC, and Ca-BTC) was studied. These Ca-MOFs had homogeneous size of microsphere structures. Generally, surface area of Ca-BDC was relatively higher than Ca-MIX and Ca-BTC, respectively. These materials were categorized as mesoporous as the pore size fall between 2 to 50 nm. Furthermore, Ca-BDC is thermally stable up to 600 ℃, while 350 ℃ for Ca-MIX and Ca-BTC. Indicated that Ca-BDC is structurally stable as compared to other two Ca-MOFs. Therefore, these materials could be possibly used for EDCs removal in water. The results showed that EE2 under this study were removed within 3 h at pH 7 and using 50 mg of each Ca-MOFs. The adsorption capacities were found to be 3.57 µg/g, 3.23 µg/g, and 3.14 µg/g for Ca-MIX, Ca-BDC, and Ca-BTC, respectively. The percentage removal follows the order Ca-MIX > Ca-BDC > Ca-BTC, which agreed well with pore size and volume. The adsorption process was best interpreted using the pseudo-second-order kinetic model and the Langmuir isotherm model, which accurately described the kinetic and equilibrium behaviors, respectively. Based on the intraparticle diffusion model, Ca-MIX and Ca-BDC samples present higher adsorption potential due to the higher surface area which allows EE2 compounds to diffused easily through adsorbents structure. The thermodynamics study revealed that the adsorption process is driven spontaneously and exhibits endothermic behavior. The initial pH solution gave a crucial influence on EE2 capture, and the neutral pH was prominent for adsorption by using Ca-MIX, while acidic condition (pH 5) for thru Ca-BTC, and alkaline condition (pH 9) by using Ca-BDC. Thus, electrostatic attraction and repulsion are the main reasons for this adsorption mechanism at various initial pH solution regarding to the pH_{pzc} and pK_a values of each Ca-MOFs and EE2. The adsorption capacity of EE2 is also influenced by the concentration of humic acid. However, at low levels of humic acid and ionic strength, these factors have minimal impact. Electrostatic and hydrophobic interactions are likely the dominant mechanisms driving EE2 adsorption onto Ca-MIX, Ca-BDC, and Ca-BTC from aqueous solutions. Corresponding to five successive cycles for Ca-MOFs regeneration, these materials show a favourable capability for the adsorption of EDCs from aqueous environment. To fully comprehend their mechanisms and the impact of different aspects on the EE2 removal, the overall interactions between EE2 and Ca-MOF must be taken into consideration.

Supplementary Information The online version contains supplementary material available at https://doi.org/10.1007/s13762-025-06564-5.

Acknowledgements This work was supported by Universiti Putra Malaysia (UPM) under Geran Putra-Inisiatif Putra Siswazah (GP-IPS/2021/9703600). The author would also like to acknowledge Graduate Research Fellowship (GRF) awarded by Universiti Putra Malaysia (UPM).

Funding Open access funding provided by The Ministry of Higher Education Malaysia and Universiti Putra Malaysia. This work was supported by the Universiti Putra Malaysia (UPM) under Geran Putra-Inisiatif Putra Siswazah (GP-IPS/2021/9703600). The author would also like to acknowledge Graduate Research Fellowship (GRF) awarded by Universiti Putra Malaysia (UPM).

Data availability The datasets used and/or analyzed during the present study are available from the corresponding author on reasonable request.

Declarations

Conflict of interest The authors declare that they have no known competing financial interests or personal relationships that could have appeared to influence the work reported in this paper.

Ethical approval and consent to participate Not applicable.

Consent for publication Not applicable.

References

Adegoke KA, Olagunju AO, Alagbada TC, Alao OC, Adesina MO, Afolabi IC, Adegoke RO, Bello OS (2022) Adsorptive removal of endocrine-disrupting chemicals from aqueous solutions: a review. Water Air Soil Pollut 233(2):38

Ahmed I, Mondol MMH, Jung MJ, Lee GH, Jhung SH (2023) MOFs with bridging or terminal hydroxo ligands: applications in adsorption, catalysis, and functionalization. Coord Chem Rev 475:214912

Alavijeh RK, Akhbari K, White J (2019) Solid–liquid conversion and carbon dioxide storage in a calcium-based metal–organic framework with micro-and nanoporous channels. Cryst Growth des 19(12):7290–7297

Almeida Â, Silva MG, Soares AM, Freitas R (2020) Concentrations levels and effects of 17alpha-ethinylestradiol in freshwater and marine waters and bivalves: a review. Environ Res 185:109316

Al-Terkawi AA, Scholz G, Emmerling F, Kemnitz E (2016) Mechanochemical synthesis, characterization, and structure determination of new alkaline earth metal-tetrafluoroterephthalate frameworks: Ca (p BDC-F4)· 4H2O, Sr (p BDC-F4)· 4H2O, and Ba (p BDC-F4). Cryst Growth des 16(4):1923–1933

Aris AZ, Shamsuddin AS, Praveena SM (2014) Occurrence of 17α-ethynylestradiol (EE2) in the environment and effect on exposed biota: a review. Environ Int 69:104–119

Aris AZ, Hir ZAM, Razak MR (2020) Metal-organic frameworks (MOFs) for the adsorptive removal of selected endocrine disrupting compounds (EDCs) from aqueous solution: a review. Appl Mater Today 21:100796

Artioli Y (2008) Adsorption. Encyclopedia of ecology, five-volume set. Elsevier, Oxford, pp 60–65. https://doi.org/10.1016/B978-008045405-4.00252-4

Bhaumik M, Agarwal S, Gupta VK, Maity A (2016) Enhanced removal of Cr (VI) from aqueous solutions using polypyrrole wrapped oxidized MWCNTs nanocomposites adsorbent. J Colloid Interface Sci 470:257–267

Bókony V, Üveges B, Ujhegyi N, Verebélyi V, Nemesházi E, Csíkvári O, Hettyey A (2018) Endocrine disruptors in breeding ponds and reproductive health of toads in agricultural, urban and natural landscapes. Sci Total Environ 634:1335–1345

Carpenter BP, Talosig AR, Rose B, Di Palma G, Patterson JP (2023) Understanding and controlling the nucleation and growth of metal–organic frameworks. Chem Soc Rev 52(20):6918–6937

Chu KH (2021) Revisiting the Temkin isotherm: dimensional inconsistency and approximate forms. Ind Eng Chem Res 60(35):13140–13147

Clouzot L, Haguenauer C, Vanrolleghem PA (2020) An extended ecosystem model for understanding EE2 indirect effects on a freshwater food web and its ecosystem function resilience. Water 12(6):1736

Couto E, Assemany PP, Carneiro GCA, Soares DCF (2022) The potential of algae and aquatic macrophytes in the pharmaceutical and personal care products (PPCPs) environmental removal: a review. Chemosphere 302:134808

da Silva LF, Nobre CR, Moreno BB, Pereira CDS, de Souza Abessa DM, Choueri RB, Gusso-Choueri PK, Cesar A (2022) Non-destructive biomarkers can reveal effects of the association of microplastics and pharmaceuticals or personal care products. Mar Pollut Bull 177:113469

de França JF, Pickler TB, Jozala AF, Dos Santos CA, Batista BL, Pedron T, Vieira RAL, Grotto D (2020) Determination of 17α-ethinylestradiol and toxic metals in surface waters, and estimation of daily intake. Environ Monit Assess 192:1–10

Dehghan A, Mohammadi AA, Yousefi M, Najafpoor AA, Shams M, Rezania S (2019) Enhanced kinetic removal of ciprofloxacin onto metal-organic frameworks by sonication, process optimization and metal leaching study. Nanomaterials 9(10):1422

Dong Y, Gai S, Zhang J, Fan R, Hu B, Wang W, Cao W, Wang J, Zhu K, Xia D, Geng L (2023) Metal-organic frameworks with mixed-ligands strategy as heterogeneous nucleation center to assist crystallization for efficient and stable perovskite solar cells. J Energy Chem 77:1–10

Esfandiari K, Mahdavi AR, Ghoreyshi AA, Jahanshahi M (2018) Optimizing parameters affecting synthetize of CuBTC using response surface methodology and development of AC@ CuBTC composite for enhanced hydrogen uptake. Int J Hydrogen Energy 43(13):6654–6665

Foo KY, Hameed BH (2010) Insights into the modeling of adsorption isotherm systems. Chem Eng J 156(1):2–10

Furukawa H, Cordova KE, O'Keeffe M, Yaghi OM (2013) The chemistry and applications of metal-organic frameworks. Science 341(6149):1230444

Garzon-Tovar L, Carné-Sánchez A, Carbonell C, Imaz I, Maspoch D (2015) Optimised room temperature, water-based synthesis of CPO-27-M metal–organic frameworks with high space-time yields. J Mater Chem A 3(41):20819–20826

George P, Das RK, Chowdhury P (2019) Facile microwave synthesis of Ca-BDC metal organic framework for adsorption and controlled release of curcumin. Microporous Mesoporous Mater 281:161–171

Gkika DA, Mitropoulos AC, Kyzas GZ (2022) Why reuse spent adsorbents? The latest challenges and limitations. Sci Total Environ 822:153612

Han J, He X, Liu J, Ming R, Lin M, Li H, Zhou X, Deng H (2022) Determining factors in the growth of MOF single crystals unveiled by in situ interface imaging. Chem 8(6):1637–1657

Hasan Z, Choi EJ, Jhung SH (2013) Adsorption of naproxen and clofibric acid over a metal–organic framework MIL-101 functionalized with acidic and basic groups. Chem Eng J 219:537–544

He J, Dai J, Zhang T, Sun J, Xie A, Tian S, Yan Y, Huo P (2016) Preparation of highly porous carbon from sustainable α-cellulose for superior removal performance of tetracycline and sulfamethazine from water. RSC Adv 6(33):28023–28033

Jamil U, Khoja AH, Liaquat R, Naqvi SR, Omar WNNW, Amin NAS (2020) Copper and calcium-based metal organic framework (MOF) catalyst for biodiesel production from waste cooking oil: a process optimization study. Energy Convers Manag 215:112934

Jun BM, Hwang HS, Heo J, Han J, Jang M, Sohn J, Park CM, Yoon Y (2019) Removal of selected endocrine-disrupting compounds using Al-based metal organic framework: performance and mechanism of competitive adsorption. J Ind Eng Chem 79:345–352

Khatoon N, Ali N, Yang H, Jun W (2024) Review of MOFs and their applications in the preparation of loose nanofiltration membranes for dye and salt fractionation. Desalin Water Treat. https://doi.org/10.1016/j.dwt.2024.100092

Kojima D, Sanada T, Wada N, Kojima K (2018) Synthesis, structure, and fluorescence properties of a calcium-based metal–organic framework. RSC Adv 8(55):31588–31593

Kul AR, Koyuncu H, Turan A, Aldemir A (2023) Comparative research of isotherm, kinetic, and thermodynamic studies for neutral red adsorption by activated carbon prepared from apple peel. Water Air Soil Pollut 234(6):383

Lee G, Ahmed I, Lee HJ, Jhung SH (2024) Adsorptive removal of organic pollutants with a specific functional group from water by using metal–organic frameworks (MOFs) or MOF-derived carbons: a review. Sep Purif Technol. https://doi.org/10.1016/j.seppur.2024.127602

Li TT, Liu YM, Wang T, Wu YL, He YL, Yang R, Zheng SR (2018) Regulation of the surface area and surface charge property of MOFs by multivariate strategy: synthesis, characterization, selective dye adsorption and separation. Microporous Mesoporous Mater 272:101–108

Li L, Guo L, Pu S, Wang J, Yang Q, Zhang Z, Yang Y, Ren Q, Alnemrat S, Bao Z (2019) A calcium-based microporous metal-organic framework for efficient adsorption separation of light hydrocarbons. Chem Eng J 358:446–455

Li Y, Wang Y, He L, Meng L, Lu H, Li X (2020) Preparation of poly (4-vinylpyridine)-functionalized magnetic Al-MOF for the removal of naproxen from aqueous solution. J Hazard Mater 383:121144

Liang PC, Liu HK, Yeh CT, Lin CH, Zima V (2011) Supramolecular assembly of calcium metal−organic frameworks with structural transformations. Cryst Growth des 11(3):699–708

Liao J, Jin B, Zhao Y, Liang Z (2019) Highly efficient and durable metal-organic framework material derived Ca-based solid sorbents for CO2 capture. Chem Eng J 372:1028–1037

Liu W, Shen X, Han Y, Liu Z, Dai W, Dutta A, Kumar A, Liu J (2019) Selective adsorption and removal of drug contaminants by using an extremely stable Cu (II)-based 3D metal-organic framework. Chemosphere 215:524–531

López-Velázquez K, Guzmán-Mar JL, Saldarriaga-Noreña HA, Murillo-Tovar MA, Hinojosa-Reyes L, Villanueva-Rodríguez M (2021) Occurrence and seasonal distribution of five selected endocrine-disrupting compounds in wastewater treatment plants of the metropolitan area of Monterrey, Mexico: the role of water quality parameters. Environ Pollut 269:116223

Łuczak J, Kroczewska M, Baluk M, Sowik J, Mazierski P, Zaleska-Medynska A (2023) Morphology control through the synthesis of metal–organic frameworks. Adv Coll Interface Sci 314:102864

Mallick A, Schön EM, Panda T, Sreenivas K, Díaz DD, Banerjee R (2012) Fine-tuning the balance between crystallization and gelation and enhancement of CO2 uptake on functionalized calcium based MOFs and metallogels. J Mater Chem 22(30):14951–14963

Martins I, Soares J, Neuparth T, Barreiro AF, Xavier C, Antunes C, Santos MM (2022) Prioritizing the effects of emerging contaminants on estuarine production under global warming scenarios. Toxics 10(2):46

Mishra P, Saxena S, Singh N, Siddique A, Joshi S (2024) Structural and mechanistic insights into the selective adsorption by metal–organic frameworks. Discov Chem 1(1):1–37

Narayanan M, El-Sheekh M, Ma Y, Pugazhendhi A, Natarajan D, Kandasamy G, Raja R, Kumar RS, Kumarasamy S, Sathiyan G, Geetha R (2022) Current status of microbes involved in the degradation of pharmaceutical and personal care products (PPCPs) pollutants in the aquatic ecosystem. Environ Pollut 300:118922

Newcombe G, Morrison J, Hepplewhite C (2002) Simultaneous adsorption of MIB and NOM onto activated carbon. I. Characterisation of the system and NOM adsorption. Carbon 40(12):2135–2146

Nguyen DTC, Le HTN, Do TS, Pham VT, Lam Tran D, Ho VTT, Tran TV, Nguyen DC, Nguyen TD, Bach LG, Ha HKP (2019) Metal-organic framework MIL-53 (Fe) as an adsorbent for ibuprofen drug removal from aqueous solutions: response surface modeling and optimization. J Chem 2019(1):5602957

Peng Y, Fang W, Krauss M, Brack W, Wang Z, Li F, Zhang X (2018) Screening hundreds of emerging organic pollutants (EOPs) in

surface water from the Yangtze river delta (YRD): occurrence, distribution, ecological risk. Environ Pollut 241:484–493
Prokić D, Vukčević M, Mitrović A, Maletić M, Kalijadis A, Janković-Častvan I, Đurkić T (2022) Adsorption of estrone, 17β-estradiol, and 17α-ethinylestradiol from water onto modified multi-walled carbon nanotubes, carbon cryogel, and carbonized hydrothermal carbon. Environ Sci Pollut Res 29:4431–4445
Puerto-Rodríguez M, López-Cartes C, Ayala R (2022) On the adsorption properties and applications of mixed-linker MOFs based on HKUST-1. J Solid State Chem 312:123260
Qu Y, Zhang C, Li F, Bo X, Liu G, Zhou Q (2009) Equilibrium and kinetics study on the adsorption of perfluorooctanoic acid from aqueous solution onto powdered activated carbon. J Hazard Mater 169(1–3):146–152
Ramzan M, Rani M, Siddiqui R, Shah AA, Arshad M, Ghauri MW, Abbas G, Yusuf K, Sillanpää M (2023) Synthesis and analytical characterization of Ca-BTC metal organic framework. Heliyon. https://doi.org/10.1016/j.heliyon.2023.e21314
Rezania S, Cho J, Nejad ZD, Barghi A, Yadav KK, Ahmed EM, Cabral-Pinto MM, Park J, Mehranzamir K (2021) Microporous metal-organic frameworks against endocrine-disruptor bisphenol A: parametric evaluation and optimization. Colloids Surf A 626:127039
Robati D (2013) Pseudo-second-order kinetic equations for modeling adsorption systems for removal of lead ions using multi-walled carbon nanotube. J Nanostruct Chem 3:1–6
Roslan MQJ, Aris AZ, Rahman MBA, Ngee LH, Isa NM, Aljafree NFA (2024) Mechanistic synthesis of a sequential calcium-carboxylate-based linker (Ca-MOFs) and rapid assessment of chemical stability through XRD analysis. J Mol Struct 1303:137566
Sargazi G, Afzali D, Mostafavi A (2018) A novel synthesis of a new thorium (IV) metal organic framework nanostructure with well controllable procedure through ultrasound assisted reverse micelle method. Ultrason Sonochem 41:234–251
Sarker M, Shin S, Jhung SH (2019) Adsorptive removal of nitroimidazole antibiotics from water using porous carbons derived from melamine-loaded MAF-6. J Hazard Mater 378:120761
Shi X, Rosa R, Lazzeri A (2010) On the coating of precipitated calcium carbonate with stearic acid in aqueous medium. Langmuir 26(11):8474–8482
Singh S, Sivaram N, Nath B, Khan NA, Singh J, Ramamurthy PC (2024) Metal organic frameworks for wastewater treatment, renewable energy and circular economy contributions. Npj Clean Water 7(1):124
Sompornpailin D, Ratanatawanate C, Chantanavorakunchai N, Punyapalakul P (2021) Effects of electrolytes and fractionated dissolved organic matter on selective adsorption of pharmaceuticals on terephthalic acid-based metal-organic frameworks. Environ Res 196:110335
Sukatis FF, Aris AZ (2021) Metal−organic frameworks based adsorbents for aquatic pollutants removal. Metal–organic frameworks for environmental remediation. American Chemical Society, pp 155–170
Sukatis FF, Wee SY, Aris AZ (2022) Potential of biocompatible calcium-based metal-organic frameworks for the removal of endocrine-disrupting compounds in aqueous environments. Water Res 218:118406
Sukatis FF, Roslan MQJ, Looi LJ, Lim HN, Rahman MBA, Aris AZ (2024) Process variables optimization for synthesizing novel calcium-based metal-organic frameworks for feasible synthetic estrogen adsorption. Microporous Mesoporous Mater 370:112822
Sumida K, Hu M, Furukawa S, Kitagawa S (2016) Structuralization of Ca2+-based metal–organic frameworks prepared via coordination replication of calcium carbonate. Inorg Chem 55(7):3700–3705
Sun X, Hu D, Yang LY, Wang N, Wang YG, Ouyang XK (2019) Efficient adsorption of Levofloxacin from aqueous solution using calcium alginate/metal organic frameworks composite beads. J Sol Gel Sci Technol 91:353–363
Tang Z, Liu ZH, Wang H, Dang Z, Liu Y (2021) A review of 17α-ethynylestradiol (EE2) in surface water across 32 countries: sources, concentrations, and potential estrogenic effects. J Environ Manag 292:112804
Tian SR, Liu YG, Liu SB, Zeng GM, Jiang LH, Tan XF, Huang XX, Yin ZH, Liu N, Li J (2018) Hydrothermal synthesis of montmorillonite/hydrochar nanocomposites and application for 17β-estradiol and 17α-ethynylestradiol removal. RSC Adv 8(8):4273–4283
Vakiti RK, Garabato BD, Schieber NP, Rucks MJ, Cao Y, Webb C, Maddox JB, Celestian A, Pan WP, Yan B (2012) Synthesis and characterization of two-and three-dimensional calcium coordination polymers built with benzene-1, 3, 5-tricarboxylate and/or pyrazine-2-carboxylate. Cryst Growth des 12(8):3937–3943
Vishnoi P, Kaleeswaran D, Kalita AC, Murugavel R (2016) Dependence of the SBU length on the size of metal ions in alkaline earth MOFs derived from a flexible C 3-symmetric tricarboxylic acid. CrystEngComm 18(47):9130–9138
Wei LQ, Lu JY, Li QQ, Zhou Y, Tang LL, Li FY (2017) A porous Ca-MOF with nano-sized Ca11 as building unit: structure, drug loading and release properties. Inorg Chem Commun 100(78):43–47
Xie J, Liu Y, Wu Y, Li L, Fang J, Lu X (2022) Occurrence, distribution and risk of pharmaceutical and personal care products in the Haihe river sediments, China. Chemosphere 302:134874
Yang J, Trickett CA, Alahmadi SB, Alshammari AS, Yaghi OM (2017) Calcium L-lactate frameworks as naturally degradable carriers for pesticides. J Am Chem Soc 139(24):8118–8121
Ye G, Chen C, Lin J, Peng X, Kumar A, Liu D, Liu J (2021) Alkali/alkaline earth-based metal–organic frameworks for biomedical applications. Dalton Trans 50(47):17438–17454
Yin Z, Liu Y, Tan X, Jiang L, Zeng G, Liu S, Tian S, Liu S, Liu N, Li M (2019) Adsorption of 17β-estradiol by a novel attapulgite/biochar nanocomposite: characteristics and influencing factors. Process Saf Environ Prot 121:155–164

Zang Y, Li LK, Zang SQ (2021) Recent development on the alkaline earth MOFs (AEMOFs). Coord Chem Rev 440:213955

Zhang X, Zhang S, Tang Y, Huang X, Pang H (2022) Recent advances and challenges of metal–organic framework/graphene-based composites. Compos B Eng 230:109532

Zhou X, Maimaitiniyazi R, Wang Y (2022) Some consideration triggered by misquotation of Temkin model and the derivation of its correct form. Arab J Chem 15(11):104267